ACS Energy LETTERS

Cite This: ACS Energy Lett. 2018, 3, 2280−2285

http://pubs.acs.org/journal/aelccp

LETTER

Synergistic In-Layer Cobalt Doping and Interlayer Iron Intercalation into Layered MnO_2 Produces an Efficient Water Oxidation Electrocatalyst

Ian G. McKendry,[‡] Loveyy J. Mohamad,[‡] Akila C. Thenuwara, Tim Marshall, Eric Borguet, Daniel R. Strongin, and Michael J. Zdilla*

Department of Chemistry, Temple University, 1901 North 13th Street, Phildadelphia, Pennsylvania 19122, United States

Supporting Information

ABSTRACT: Described is a synthetic method to enhance the electrocatalytic activity of the layered manganese oxide, birnessite, for the oxygen evolution reaction (OER) through the development of a Mn/Co/Fe ternary phase. The ternary phase was synthesized by the simultaneous doping of Co^{3+} into the manganese oxide lattice and intercalation of Fe^{2+} within the interlayer region of birnessite ($K_xFe[Co_{0.16}Mn_{0.84}O_2]$). The material was characterized by X-ray diffractometry, electron microscopy, X-ray photoelectron, energy dispersive, and Raman spectroscopies and electrochemical analysis. The $K_xFe[Co_{0.16}Mn_{0.84}O_2]$ material demonstrated efficient OER electrocatalysis with an overpotential (η) of 375 mV (at 10 mA/cm^2) and Tafel slope (b) of 56 mV/dec, surpassing the catalytic activity of both standard potassium birnessite ($\eta \approx 800$ mV, $b = 240$ mV/dec) and cobalt-doped birnessite with a Co:Mn ratio of 1:5 ($\eta \approx 750$ mV, $b = 230$ mV/dec) and with a catalytic lifetime 150-fold greater than that of standard birnessite and 100-fold greater than that of the iron-free cobalt-doped birnessite at 5 mA/cm^2.

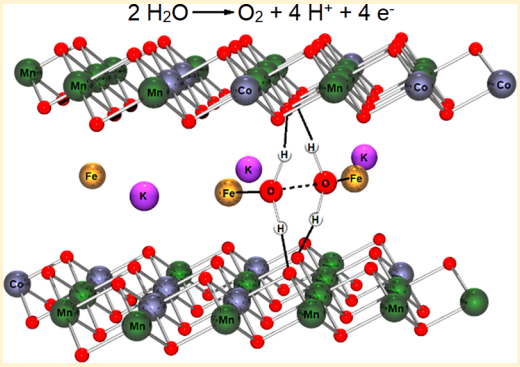

Reliance on combustible fossil fuels (natural gas, oil, coal, etc.) as a prominent source of energy carries the risk of increased emissions of undesirable greenhouse gases such as carbon dioxide. In turn, mankind's need for energy is leading to undesirable climate effects, such as sea-level rise, ocean acidification, and changes in river flow.[1,2] In order to attenuate undesirable and irreversible climate changes, it is essential to find clean, renewable sources of energy. Nonfossil-fuel-based solar power stands as a cornerstone future energy source.[3] While solar power is a viable energy source, the lack of efficient, long-term storage remains a significant hurdle for its large-scale suitability.

Solar hydrogen is a promising storage method due to the advances in hydrogen fuel cell technology and the abundance of water and sunlight.[4,5] However, water splitting poses a significant challenge because the reaction is thermodynamically uphill and kinetically hindered, particularly with regard to the oxidation of water to O_2. The minimum potential for water oxidation is +1.23 V (at pH 0, 25 °C) vs the standard hydrogen electrode (SHE) with a free energy of 237 kJ/mol for the whole process under standard conditions.[6,7]

$$H_2O_{(l)} \rightarrow \frac{1}{2}O_{2(g)} + H_{2(g)} \qquad \Delta G^\circ = 237 \text{ kJ/mol}$$

The high activation energy required to facilitate the splitting of water can most efficiently be overcome through the development of stable water oxidation catalysts comprising cheap, earth-abundant elements. Although precious metal oxides, such as ruthenium and iridium, have proven to be catalytically efficient in lowering the activation barrier for water oxidation,[8] their high cost and rarity make them unfeasible on an industrial scale. Therefore, the development of cheap efficient catalysts continues to be an active area of study.[9]

Stable, cheap, and earth-abundant elements that are prime candidates for water oxidation catalysis include first-row transition metal elements such as Ni, Co, Fe, Cu, and Mn as well as their oxides and hydroxides.[10−15] One metal oxide system of interest is birnessite, a 2D-layered material composed of edge-sharing octahedra (MnO_6).[16−18] Compris-

Received: July 12, 2018
Accepted: August 14, 2018
Published: August 14, 2018

Downloaded via TEMPLE UNIV on January 8, 2025 at 19:52:32 (UTC).
See https://pubs.acs.org/sharingguidelines for options on how to legitimately share published articles.

© 2018 American Chemical Society

DOI: 10.1021/acsenergylett.8b01217
ACS Energy Lett. 2018, 3, 2280−2285

ing the edge-sharing octahedra is a mixture of Mn^{3+} and Mn^{4+}. The Mn^{3+} defects result in a manganese oxide lattice with a net negative charge. Water molecules and positively charged cations (such as K^+ and Na^+), which maintain charge neutrality, are confined in the interlayer region, providing structural stability.[17−20] While manganese oxide-based systems have been demonstrated to be less catalytically active than ruthenium- and iridium-bearing systems,[9] studies have focused on enhancing the activity of 2D-layered manganese oxides by modifying the internal and external structural features.[9,13,18,21−24]

Modifications to the manganese oxide lattice have been widely studied with regards to birnessite. Incorporation of Mn^{3+} species has shown to be an efficient method to enhance the water oxidation activity of the material.[14,16,25−27] As a separate consideration, doping the manganese oxide sheets with Ni and Co can effectively modify the chemical properties of the birnessite material.[23,28,29] Previous work by our group has demonstrated that incorporation of Co^{3+} into the sheets enhances charge mobility through the system with residual interstitial Co^{3+} in the interlayer facilitating an important catalytic function for water oxidation.[29]

In addition to the manganese oxide lattice features, recent work has focused on the role of interlayer cations.[25,29−34] Initial work from Kurz and co-workers demonstrated a correlation between the interlayer cation and activity. Through the intercalation of various Lewis acidic alkali and alkaline earth cations, Ca^{2+} and Sr^{2+} were found to much more efficiently facilitate the Oxygen Evolution Reaction (OER) in the presence of a chemical oxidant.[35] This correlation matches well with similar substitution studies performed in the Mn-bearing oxygen-evolving complex (OEC) in photosystem II.[35−37] In recent computational worfapproach segregates in-layer dopants of one element typek by Lucht and Mendoza-Coretz, the interlayer cations were shown to play a role in tuning the electronic structure of the birnessite material. Changes in the calculated band structure and density of states were observed when these cations were exchanged.[38]

Computational and experimental collaborative efforts in our group have revealed some of the special features of the birnessite interlayer. Molecular dynamics simulations have demonstrated the unique frustration effects and orientation of interlayer substrate waters. These effects lower the activation energy required in solvent-mediated electron transfer processes like water oxidation catalysis.[39] This is supported by experimental work focused on populating the interlayer with OER-active cations, Ni^{2+} and Co^{2+}, where a reduction in the electrocatalytic overpotential needed for OER catalysis was lowered from 770 mV (at 10 mA/cm^2, pH 14) to 400 and 360 mV (at 10 mA/cm^2, pH 14), respectively.[31,33] Further, tuning of band structures of the MnO_2 lattice by incorporation of Mn^{3+} or Co^{3+} benefits catalysis by providing low-effective-mass oxidizing equivalents.[14,29,38]

In this study, we combine the advantages of electronic structure tuning by lattice doping and interlayer-frustration-mediated redox catalysis using intercalation procedures to confine iron complexes within cobalt-doped birnessite, producing a new ternary Mn/Co/Fe layered metal oxide material, $K_xFe[Co_{0.16}Mn_{0.84}O_2]$, where the elements outside of the brackets refer to intercalated ions and the elements inside of the brackets refer to the metal oxide layers. A novelty of the approach is the segregation of in-layer dopants of one element type (cobalt) from interlayer intercalants of another type

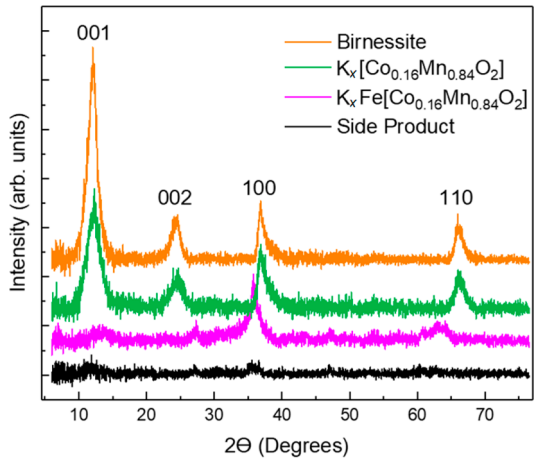

Figure 1. XRD patterns of standard potassium birnessite, $K[Co_{0.16}Mn_{0.84}O_2]$, $Fe[Co_{0.16}Mn_{0.84}O_2]$, and side product identified as magnetite and lepidocrocite iron oxyhydroxides.

(iron). A synergistic effect is uncovered where the ternary material is capable of more efficient OER catalysis than either of the binary materials. In this contribution, we report on the synthetic protocols for intercalating iron, the new ternary iron-intercalated cobalt−manganese dioxide system, the iron oxyhydroxide side products formed, and the importance of interlayer vs in-layer dopants.

Synthetic parent, cobalt-doped, and iron-intercalated birnessites were synthesized,[31,40,41] and XRD, TEM, SEM, Raman, ICP, and XPS were used to characterize the ternary iron-intercalated, cobalt-doped birnessite particles. In comparison to regular and cobalt-doped birnessites, XRD (Figures 1 and S1) shows a significant reduction in the intensities of the 001 and 002 peaks in the in the $K_xFe[Co_{0.16}Mn_{0.84}O_2]$ material, suggesting an increased stacking disorder caused by the incorporation of confined metal ions after the intercalation procedure was performed.[23,29,41] Furthermore, the increase in intensity of the 002 signal with respect to the 001 signal in the $K_xFe[Co_{0.16}Mn_{0.84}O_2]$ material (as compared to the 002:001 ratio of birnessite) is indicative of the replacement of potassium with a stronger scattering ion in the interlayer region. The increase in intensity along with the shift of the 001 and 002 peaks to higher angles is consistent with the presence of iron in the interlayer region of the material.[31] Determination of the stoichiometric ratios of the metal elements (Figure S2) shows that the molar ratio of iron is at near unity with the other transition metals, suggesting the incorporation of quite a lot of iron, and is likely responsible for the extensive stacking disorder. The shift of the 110 signal to a lower angle suggests the expansion of the hexagonal MO_2 layers, most likely by partial reduction of the MnO_2 lattice in the presence of the Fe-hydrazine complex, which balances the positive charge of the incorporated iron ions. The presence of interlayer metal ions is also observed in the Raman spectra (Figures 2 and S3) with an increase in the M−O out-of-plane stretching mode at 640 cm^{-1} relative to the in-plane stretching mode at 570 cm^{-1}.[42] The sharpening and intensifying of the peak at 250 cm^{-1} (Figure 2) suggests additional Fe−O modes resulting from Fe in the interlayer as an iron-oxo complex as opposed to solvated Fe^{2+} ions.

Further analysis of the particles by TEM shows the transformation of the microsized Co-birnessite particles (Figures 3 and S4) to a less densely packed morphology of

DOI: 10.1021/acsenergylett.8b01217
ACS Energy Lett. 2018, 3, 2280−2285

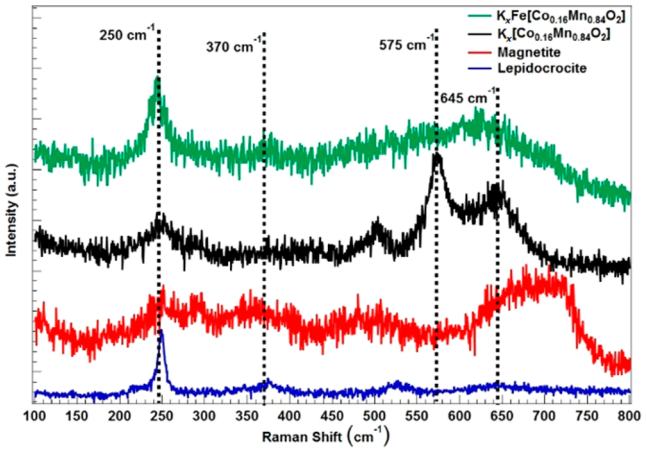

Figure 2. Raman spectra of cobalt-doped birnessite,[29] $K_xFe[Co_{0.16}Mn_{0.84}O_2]$, magnetite ($Fe_3O_4$), and lepidocrocite (Fe(O)(OH)) side products.

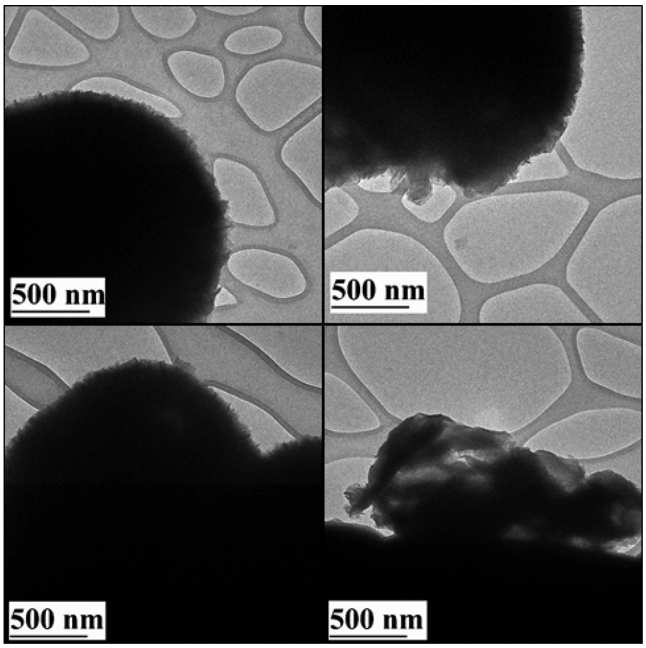

Figure 3. TEM images of cobalt-doped birnessite before iron intercalation.

birnessite particles with fewer layers after the iron intercalation procedure was performed (Figure S6). This transformation can be further observed in the surface area measurements (Table S1) with an increase in total surface area from 3.8 to 145 m^2/g after iron intercalation. Additional TEM and SEM analysis (Figures S5 and S8) indicates the significant presence of a nanoparticulate side product (particles ~10−20 nm) that persisted even after multiple washings.

Analysis of the side product with XRD (Figure S2a) revealed a combination of magnetite [Fe_3O_4] and lepidocrocite [γ-Fe(O)(OH)] phase iron byproducts.[43,44] STEM-EDS (Figure S11) confirmed that these side products were primarily iron-oxide-based,[45] though traces of cobalt and manganese contaminants were present. For the bulk birnessite-based product, EDS mappings (Figures S9 and S10) showed these metal atoms to be evenly dispersed throughout the $K_xFe[Co_{0.16}Mn_{0.84}O_2]$ particles. Analysis of composition of the material with XPS (Figures S12a.b and S13a.b) showed good agreement with the XRD- and TEM-based assignments of $K_xFe[Co_{0.16}Mn_{0.84}O_2]$ with Fe_3O_4 and γ-Fe(O)(OH) contaminants.[46] In particular, the O 1s region supports the presence of an oxyhydroxide contaminant material, assignable to Fe_3O_4 and γ-Fe(O)(OH). Upon washing the $K_xFe[Co_{0.16}Mn_{0.84}O_2]$ sample with 15 mL of water 10−15 times and centrifugation, the amount of side product present was greatly reduced though not fully eliminated. XPS analysis (Figures S12e and S13e) shows a significant change in the oxygen character with metal-oxo character at 528 eV as the predominant peak. Furthermore, when fitting the Fe $2p_{3/2}$ (Figures S12d and S13f) region with two peaks representing $Fe^{2+/3+}$, a significant growth in the Fe^{2+} character is observed.[47] This suggests the loss of the iron oxyhydroxide side product and the presence of interlayer Fe^{2+}.

After Washing, TEM and SEM (Figures S6 and S8) confirm the significant reduction of the side product phase with the majority of particles observed possessing a "wrinkled paper" morphology like that seen in hexagonal phase standard birnessite.[16,31] However, a significant reduction in both the lateral dimension and total layer number is observed in the remaining birnessite-like nanoparticles. In previous work, it was hypothesized that hydrazine helped shuttle nickel into the interlayer of birnessite.[31] However, excess hydrazine in solution and residual hydrazine ligand post-intercalation can result in the reduction and dissolution of Mn^{2+}.

It is important to consider the role that Fe^{2+} plays in the formation of the nanophase and iron oxyhydroxide side products, as such analogous nickel- or cobalt-based side products were not observed in previous nickel- and cobalt-intercalated birnessite experiments.[31,33] While an exact mechanism was not elucidated, the more reactive Fe^{2+} (vs Ni^{2+}) likely plays a significant role in the transformation to the nanophase and subsequent side product formation. We hypothesize that excess Fe-hydrazine in solution precipitates out as either magnetite or lepidocrocite, providing reducing equivalents for birnessite. These reducing equivalents and possibly those from excess hydrazine reduce the Co-birnessite surface, causing the dissolution of Mn^{2+}, expanding the MnO_2 lattice (Figure 1), and giving the nanoparticulate birnessite and Fe byproducts. Additionally, the presence of iron-oxo complexes in the interlayer may further aid in exfoliation and transformation of the bulk to nanophase material.

To test this hypothesis, two solutions of Fe^{2+} were allowed to oxidize in air for 8 h: one Fe^{2+} solution contained hydrazine (redox-active ligand), and the other contained ammonia (non-redox-active ligand). In each case, precipitate formation was observed, consistent with the hypothesis that the Fe-based side product forms via the decomposition of the Fe-hydrazine interlayer shuttling complex. To our surprise, we found the selective precipitation of magnetite from ammonia-containing solution and lepidocrocite from hydrazine-containing solution, as confirmed through XRD (Figure S2) and TEM (Figure S7).

The 1:5 Co:Mn doped birnessite and $K_xFe[Co_{0.16}Mn_{0.84}O_2]$ were tested for their electrochemical OER activity using a standard three-electrode configuration at pH 14, as outlined in the methods section. The catalyst was deposited as an ink with carbon powder and naffion as electronically and ionically conductive binders. The overpotential for the modified $K_xFe[Co_{0.16}Mn_{0.84}O_2]$ material was significantly lowered (from 750 to 375 mV) after the intercalation procedure. Furthermore, the Tafel slope decreased from 240 (birnessite)[29]

DOI: 10.1021/acsenergylett.8b01217
ACS Energy Lett. 2018, 3, 2280−2285

to 56 mV/dec ($K_xFe[Co_{0.16}Mn_{0.84}O_2]$, Figure S19). Chronopotentiometry shows a significant 100-fold improvement in the total lifetime after transformation of Co-birnessite (12.5 min) to $K_xFe[Co_{0.16}Mn_{0.84}O_2]$ (>12.5 h), and a 150-fold improvement over that of parent birnessite (5 min)[32] at the same current density (Figure S18) with reproducible behavior across several preparations (Figures S15 and S18). In birnessites, catalyst death occurs presumably by the loss of active site activity, rather than the destruction of the birnessite phase, which remains intact in the dead catalyst based on XRD analysis.[16,31]

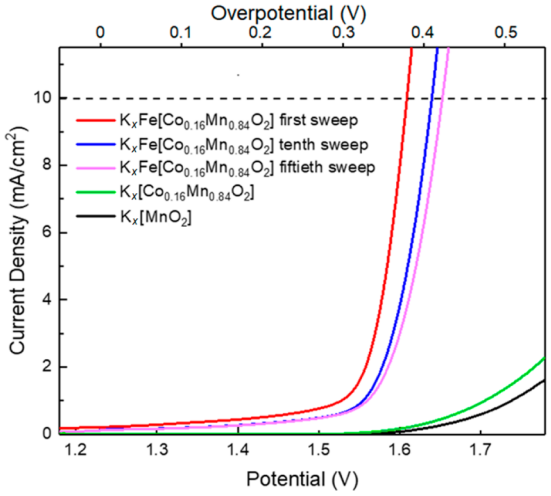

Figure 4. Catalytic current measurement by LSV on synthesized catalysts vs potential vs SHE.

The presence of a contaminant nanophase is an important consideration when examining catalytic activity, especially considering that the first linear sweep voltammetry (LSV) sweep (in Figure 4) represents the lowest overpotential, with the overpotential decreasing slightly on subsequent sweeps. This may be due to highly active catalytic active sites at the surface that do not survive the first sweep or to the presence of the contaminant nanophase, which could be more active than the birnessite phase. To verify that the observed reduction in overpotential was not attributable to the presence of this residual side product, magnetite (Fe_3O_4) and lepidocrocite [γ-Fe(O)(OH)] were selectively synthesized, characterized, and analyzed via electrochemistry. Electrochemical studies showed that the magnetite and lepidocrocite phases both gave an overpotential of 660 mV. Thus, the lower 375 mV cannot be attributed to the presence of the iron oxyhydroxide side contaminant species (Figure S17). Recent work by Gray and co-workers has demonstrated the ability of iron to handle the oxidative demands of water oxidation.[48]

To further support the importance of interlayer Fe in the enhancement of catalytic activity, a separate layer-by-layer assembly method was used to controllably assemble Co-birnessite sheets with interlayer Fe^{2+} (Figure S14). This synthesis strategy was accomplished through the alternate dipping of a conductive FTO glass electrode between a suspension of negatively charged monolayer nanosheets (MnO_2^{x-} or $Co_{0.3}Mn_{0.7}O_2^{x-}$) and cationic (K^+ or K^+/Fe^{2+}) solution. This procedure yielded four different permutations of assembled catalysts from sheets with or without cobalt and with interlayer regions with or without iron: $K_x[MnO_2]$, $K_xFe[MnO_2]$, $K_x[Co_{0.3}Mn_{0.7}O_2]$, and $K_xFe[Co_{0.3}Mn_{0.7}O_2]$. Electrocatalytic OER activity (Figures 5 and S16) was tested for each assembled catalyst. Through this experiment, the same trend in overpotential was observed that indicates the importance of both the presence of an interlayer iron intercalant and an in-layer cobalt dopant: $K_x[MnO_2]$ (η = 1.10 V) > $K_x[Co_{0.3}Mn_{0.7}O_2]$ (η = 0.72 V) > $K_xFe[MnO_2]$ (η = 0.66 V) > $K_xFe[Co_{0.3}Mn_{0.7}O_2]$ (η = 0.56 V). However, the layer-by-layer assembled catalysts did not show the same low overpotential as the synthetic catalysts most likely due to a decreased defect density for these well-controlled layer-deposited materials. Further, the electrical contact between the FTO and the catalyst may be impeded by the PEI layer used as adhesive.

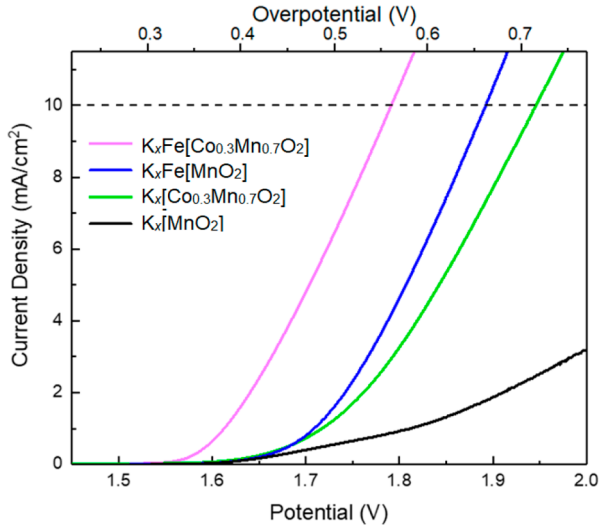

Figure 5. Catalytic current measurement by LSV on layer-by-layer assembled catalysts vs potential vs SHE.

In conclusion, we report an efficient method to enhance the catalytic activity of layered manganese oxides through the cooperative doping of the 2D lattice and interlayer. Doping the MnO_2 lattice with cobalt enhances the conductivity of the MnO_2 sheets, allowing for holes to be more efficiently delivered to the interlayer iron oxide active site. In addition to the formation of the ternary $K_xFe[Co_{0.16}Mn_{0.84}O_2]$ material, the iron hydrazine intercalation procedure decreases the particle size and increases the concentration of Mn^{3+} defects. The increase in the particle surface area and porosity may enhance the rate at which substrate water is shuttled into the interlayer active sites for the diffusion-limited process. With the inclusion of both in-layer cobalt and interlayer iron, a highly efficient OER catalyst is obtained whose overpotential drops by 425 mV and whose Tafel slope drops by 184 mV/decade (η = 375 mV, b = 56 mV/dec) with respect to pure birnessite and which is stable under operation for over 11 h, 100× longer than the iron-free cobalt-doped birnessite sample and 150× longer than standard birnessite.[32]

■ ASSOCIATED CONTENT

Supporting Information

The Supporting Information is available free of charge on the ACS Publications website at DOI: 10.1021/acsenergylett.8b01217.

DOI: 10.1021/acsenergylett.8b01217
ACS Energy Lett. 2018, 3, 2280−2285

Experimental procedures, X-ray powder patterns, Raman spectra and reference spectra,[49] electron micrographs, EDS and XPS spectra, details on nanosheet assembly and characterization, additional electrochemical data, chronopotentiometry, and details of BET surface area analysis (PDF)

AUTHOR INFORMATION

Corresponding Author

*E-mail: mzdilla@temple.edu.

ORCID

Akila C. Thenuwara: 0000-0002-6146-9238
Daniel R. Strongin: 0000-0002-1776-5574
Michael J. Zdilla: 0000-0003-0212-2557

Author Contributions

‡I.G.M. and L.J.M. contributed equally.

Notes

The authors declare no competing financial interest.

ACKNOWLEDGMENTS

This work was supported by the Center for the Computational Design of Functional Layered Materials, an EnergyFrontier Research Center funded by the U.S. Department of Energy, Office of Science, Basic Energy Sciences, under Award # DE-SC0012575. The XPS measurements carried out at the University of Delaware surface analysis facility were supported by the NSF (1428149) and the NIH NIGMS COBRE program (P30-GM110758). The authors gratefully acknowledge Yaroslav Aulin for assistance with Raman spectroscopy and Mykola Seredych and Yuri Gogotsi for use and assistance with BET surface area measurements at Drexel University.

REFERENCES

(1) Appel, A. M.; Bercaw, J. E.; Bocarsly, A. B.; Dobbek, H.; DuBois, D. L.; Kenis, P. J. A.; Dupuis, M.; Ferry, J. G.; Fujita, E.; Hille, R.; et al. Frontiers, Opportunities, and Challenges in Biochemical and Chemical Catalysis of CO_2 Fixation. *Chem. Rev.* **2013**, *113*, 6621−6658.

(2) Xu, D.; Wang, D.; Li, B.; Fan, X.; Zhang, X. W.; Ye, N. H.; Wang, Y.; Mou, S.; Zhuang, Z. Effects of CO2 and Seawater Acidification on the Early Stages of Saccharina japonica Development. *Environ. Sci. Technol.* **2015**, *49*, 3548−3556.

(3) Walter, M. G.; Warren, E. L.; McKone, J. R.; Boettcher, S. W.; Mi, Q.; Santori, E. A.; Lewis, N. S. Solar Water Splitting Cells. *Chem. Rev.* **2010**, *110*, 6446−6473.

(4) Bak, T.; Nowotny, J.; Rekas, M.; Sorrell, C. C. Photo-Electrochemical Hydrogen Generation from Water Using Solar Energy. Materials-related aspects. *Int. J. Hydrogen Energy* **2002**, *27*, 991−1022.

(5) Ananyev, G.; Dismukes, G. C. How Fast Can Photosystem II Split Water? Kinetic performance at high and low frequencies. *Photosynth. Res.* **2005**, *84*, 355−365.

(6) Kanan, M. W.; Nocera, D. G. In Situ Formation of an Oxygen-Evolving Catalyst in Neutral Water Containing Phosphate and Co^{2+}. *Science* **2008**, *321*, 1072−1075.

(7) Bard, A. J.; Fox, M. A. Artificial Photosynthesis: Solar Splitting of Water to Hydrogen and Oxygen. *Acc. Chem. Res.* **1995**, *28*, 141−145.

(8) Gorlin, Y.; Jaramillo, T. A Bifunctional Nonprecious Metal Catalyst for Oxygen Reduction and Water Oxidation. *J. Am. Chem. Soc.* **2010**, *132*, 13612−13614.

(9) Pinaud, B. A.; Chen, Z.; Abram, D. N.; Jaramillo, T. F. Thin Films of Sodium Birnessite-Type MnO_2: Optical Properties, Electronic Band Structure, and Solar Photoelectrochemistry. *J. Phys. Chem. C* **2011**, *115*, 11830−11838.

(10) Hurst, J. K. In Pursuit of Water Oxidation Catalysts for Solar Fuel Production. *Science* **2010**, *328*, 315−316.

(11) McAlpin, J. G.; Stich, T. a.; Casey, W. H.; Britt, R. D. Comparison of Cobalt and Manganese in the Chemistry of Water Oxidation. *Coord. Chem. Rev.* **2012**, *256*, 2445−2452.

(12) Pokhrel, R.; Brudvig, G. W. Oxygen-Evolving Complex of Photosystem II: Correlating Structure with Spectroscopy. *Phys. Chem. Chem. Phys.* **2014**, *16*, 11812.

(13) Wiechen, M.; Najafpour, M. M.; Allakhverdiev, S. I.; Spiccia, L. Water Oxidation Catalysis by Manganese Oxides: Learning from Evolution. *Energy Environ. Sci.* **2014**, *7*, 2203.

(14) Maitra, U.; Naidu, B. S.; Govindaraj, A.; Rao, C. N. R. Importance of Trivalency and the eg^1 Configuration in the Photocatalytic Oxidation of Water by Mn and Co oxides. *Proc. Natl. Acad. Sci. U. S. A.* **2013**, *110*, 11704−11505.

(15) Du, P.; Eisenberg, R. Catalysts Made of Earth-Abundant Elements (Co, Ni, Fe) for Water Splitting: Recent Progress and Future Challenges. *Energy Environ. Sci.* **2012**, *5*, 6012.

(16) McKendry, I. G.; Kondaveeti, S. K.; Shumlas, S. L.; Strongin, D. R.; Zdilla, M. J. Decoration of the Layered Manganese Oxide Birnessite with Mn (II/III) Gives a New Water Oxidation Catalyst with Fifty-Fold Turnover Number Enhancement. *Dalton Trans* **2015**, *44*, 12981−12984.

(17) Post, J. E. Manganese oxide minerals: Crystal Structures and Economic and Environmental Significance. *Proc. Natl. Acad. Sci. U. S. A.* **1999**, *96*, 3447−3454.

(18) Kwon, K. D.; Refson, K.; Sposito, G. On the Role of Mn (IV) Vacancies in the Photoreductive Dissolution of Hexagonal Birnessite. *Geochim. Cosmochim. Acta* **2009**, *73*, 4142−4150.

(19) Tebo, B. M.; Bargar, J. R.; Clement, B. G.; Dick, G. J.; Murray, K. J.; Parker, D.; Verity, R.; Webb, S. M. Biogenic Manganese Oxides: Properties and Mechanisms of Formation. *Annu. Rev. Earth Planet. Sci.* **2004**, *32*, 287−328.

(20) Giovanoli, R. A. Review of the Todorokite-Buserite Problem: Implications to the Mineralogy of Marine Manganese Nodules. *Am. Mineral.* **1985**, *70*, 202−204.

(21) Frey, C. E.; Wiechen, M.; Kurz, P. Water-Oxidation Catalysis by Synthetic Manganese Oxides−Systematic Variations of the Calcium Birnessite Theme. *Dalt. Trans.* **2014**, *43*, 4370−4379.

(22) Najafpour, M. M.; Sedigh, D. J. Water Oxidation by Manganese Oxides, a New Step Towards a Complete Picture: Simplicity is the Ultimate Sophistication. *Dalt. Trans.* **2013**, *42* (34), 12173.

(23) Yin, H.; Li, H.; Wang, Y.; Ginder-Vogel, M.; Qiu, G.; Feng, X.; Zheng, L.; Liu, F. Effects of Co and Ni Co-Doping on the Structure and Reactivity of Hexagonal Birnessite. *Chem. Geol.* **2014**, *381*, 10−20.

(24) Najafpour, M. M.; Moghaddam, A. N. Amorphous Manganese Oxide-Coated Montmorillonite as an Efficient Catalyst for Water Oxidation. *New J. Chem.* **2012**, *36*, 2514.

(25) Takashima, T.; Hashimoto, K.; Nakamura, R. Mechanisms of pH-Dependent Activity for Water Oxidation to Molecular Oxygen by MnO_2 Electrocatalysts. *J. Am. Chem. Soc.* **2012**, *134*, 1519−1527.

(26) Robinson, D. M.; Go, Y. B.; Mui, M.; Gardner, G.; Zhang, Z.; Mastrogiovanni, D.; Garfunkel, E.; Li, J.; Greenblatt, M.; Dismukes, G. C. Photochemical Water Oxidation by Crystalline Polymorphs of Manganese Oxides: Structural Requirements for Catalysis. *J. Am. Chem. Soc.* **2013**, *135*, 3494−3501.

(27) Peng, H.; McKendry, I. G.; Ding, R.; Thenuwara, A. C.; Kang, Q.; Shumlas, S. L.; Strongin, D. R.; Zdilla, M. J.; Perdew, J. P. Redox Properties of Birnessite from a Defect Perspective. *Proc. Natl. Acad. Sci. U. S. A.* **2017**, *114*, 9523−9528.

(28) Yin, H.; Tan, W.; Zheng, L.; Cui, H.; Qiu, G.; Liu, F.; Feng, X. Characterization of Ni-Rich Hexagonal Birnessite and its Geochemical Effects on Aqueous Pb^{2+}/Zn^{2+} and As (III). *Geochim. Cosmochim. Acta* **2012**, *93*, 47−62.

(29) Mckendry, I. G.; Thenuwara, A. C.; Shumlas, S. L.; Peng, H.; Aulin, Y. V.; Chinnam, P. R.; Borguet, E.; Strongin, D. R.; Zdilla, M. J. Systematic Doping of Cobalt into Layered Manganese Oxide Sheets

DOI: 10.1021/acsenergylett.8b01217
ACS Energy Lett. 2018, 3, 2280−2285

Substantially Enhances Water Oxidation Catalysis. *Inorg. Chem.* **2018**, *57*, 557−564.
(30) Birkner, N.; Nayeri, S.; Pashaei, B.; Najafpour, M. M.; Casey, W. H.; Navrotsky, A. Energetic Basis of Catalytic Activity of Layered Nanophase Calcium Manganese Oxides for Water Oxidation. *Proc. Natl. Acad. Sci. U. S. A.* **2013**, *110*, 8801−8806.
(31) Thenuwara, A. C.; Cerkez, E. B.; Shumlas, S. L.; Attanayake, N. H.; McKendry, I. G.; Frazer, L.; Borguet, E.; Kang, Q.; Remsing, R. C.; Klein.; et al. Nickel Confined in the Interlayer Region of Birnessite: an Active Electrocatalyst for Water Oxidation. *Angew. Chem., Int. Ed.* **2016**, *55*, 10381−10385.
(32) Thenuwara, A. C.; Shumlas, S. L.; Attanayake, N. H.; Cerkez, E. B.; McKendry, I. G.; Frazer, L.; Borguet, E.; Kang, Q.; Zdilla, M. J.; Sun, J.; et al. Copper-Intercalated Birnessite as a Water Oxidation Catalyst. *Langmuir* **2015**, *31*, 12807−12813.
(33) Thenuwara, A. C.; Shumlas, S. L.; Attanayake, N. H.; Aulin, Y. V.; McKendry, I. G.; Qiao, Q.; Zhu, Y.; Borguet, E.; Zdilla, M. J.; Strongin, D. R. Intercalation of Cobalt into the Interlayer of Birnessite Improves Oxygen Evolution Catalysis. *ACS Catal.* **2016**, *6*, 7739−7743.
(34) Najafpour, M. M.; Isaloo, M. A.; Ghobadi, M. Z.; Amini, E.; Haghighi, B. The Effect of Different Metal Ions Between Nanolayers of Manganese Oxide on Water Oxidation. *J. Photochem. Photobiol., B* **2014**, *141*, 247−252.
(35) Wiechen, M.; Zaharieva, I.; Dau, H.; Kurz, P. Layered Manganese Oxides for Water-Oxidation: Alkaline Earth Cations Influence Catalytic Activity in a Photosystem II-Like Fashion. *Chem. Sci.* **2012**, *3*, 2330.
(36) Ono, T.-a.; Inoue, Y. Discrete Extraction of the Ca Atom Functional for O_2 Evolution in Higher Plant Photosystem II by a Simple Low pH Treatment. *FEBS Lett.* **1988**, *227*, 147−152.
(37) Preston, C.; Critchley, C. Ca^{2+} Requirement for Photosynthetic Oxygen Evolution of Spinach and Mangrove Photosytsem II Membrane Preparations. *FEBS Lett.* **1985**, *184*, 318−322.
(38) Lucht, K. P.; Mendoza-Cortes, J. L. Birnessite: A Layered Manganese Oxide to Capture Sunlight for Water-Splitting Catalysis. *J. Phys. Chem. C* **2015**, *119*, 22838−22846.
(39) Remsing, R. C.; McKendry, I. G.; Strongin, D. R.; Klein, M. L.; Zdilla, M. J. Frustrated Solvation Structures Can Enhance Electron Transfer Rates. *J. Phys. Chem. Lett.* **2015**, *6*, 4804−4808.
(40) McKenzie, R. The synthesis of Birnessite, Cryptomelane, and Some Other Oxides and Hydroxides of Manganese. M. *Mineral. Mag.* **1971**, *38*, 493−502.
(41) Zhao, W.; Cui, H.; Liu, F.; Tan, W.; Feng, X. Relationship Between Pb^{2+} Adsorption and Average Mn Oxidation State in Synthetic Birnessites. *Clays Clay Miner.* **2009**, *57* (5), 513−520.
(42) Julien, C.; Massot, M.; Baddour-Hadjean, R.; Franger, S.; Bach, S.; Pereira-Ramos, J. P. Raman Spectra of Birnessite Manganese Dioxides. *Solid State Ionics* **2003**, *159*, 345−356.
(43) Haavik, C.; Stølen, S.; Fjellvåg, H.; Hanfland, M.; Häusermann, D. Equation of State of Magnetite and Its High-Pressure Modification: Thermodynamics of the Fe-O System at High Pressure. *Am. Mineral.* **2000**, *85*, 514−523.
(44) Liu, A.; Liu, J.; Pan, B.; Zhang, W. Formation of Lepidocrocite (γ-FeOOH) from Oxidation of Nanoscale Zero-Valent Iron (nZVI) in Oxygenated Water. *RSC Adv.* **2014**, *4*, 57377−57382.
(45) Shi, H.; Liang, H.; Ming, F.; Wang, Z. Efficient Overall Water-Splitting Electrocatalysis Using Lepidocrocite VOOH Hollow Nanospheres. *Angew. Chem., Int. Ed.* **2017**, *56*, 573−577.
(46) Grosvenor, A. P.; Kobe, B. A.; Biesinger, M. C.; McIntyre, N. S. Investigation of Multiplet Splitting of Fe 2p XPS Spectra and Bonding in Iron Compounds. *Surf. Interface Anal.* **2004**, *36*, 1564−1574.
(47) Aronniemi, M.; Lahtinen, J.; Hautojärvi, P. Characterization of Iron Oxide Thin Films. *Surf. Interface Anal.* **2004**, *36*, 1004−1006.
(48) Hunter, B. M.; Thompson, N. B.; Müller, A. M.; Rossman, G. R.; Hill, M. G.; Winkler, J. R.; Gray, H. B. Trapping an Iron(VI) Water-Splitting Intermediate in Nonaqueous Media. *Joule* **2018**, *2*, 747−763.
(49) Lafuente, B.; Downs, R. T.; Yang, H.; Stone, N. The Power of Databases: the RRUFF Project. In *Highlights in Mineralogical Crystallography*; Armbruster, T., Danisi, R M., Eds.; 2015.

DOI: 10.1021/acsenergylett.8b01217
ACS Energy Lett. 2018, 3, 2280−2285